



# Modeling reactive transport of reclaimed water through large soil columns with different low-permeability layers

Haizhu Hu · Xiaomin Mao · D. A. Barry ·  
Chengcheng Liu · Pengxiang Li

**Abstract** The efficacy of different proportions of silt-loam/bentonite mixtures overlying a vadose zone in controlling solute leaching to groundwater was quantified. Laboratory experiments were carried out using three large soil columns, each packed with 200-cm-thick riverbed soil covered by a 2-cm-thick bentonite/silt-loam mixture as the low-permeability layer (with bentonite mass accounting for 12, 16 and 19 % of the total mass of the mixture). Reclaimed water containing ammonium ( $\text{NH}_4^+$ ), nitrate ( $\text{NO}_3^-$ ), organic matter (OM), various types of phosphorus and other inorganic salts was applied as inflow. A one-dimensional mobile-immobile multi-species reactive transport model was used to predict the preferential flow and transport of typical pollutants through the soil columns. The simulated results show that the model is able to predict the solute transport in such conditions. Increasing the amount of bentonite in the low-permeability layer improves the removal of  $\text{NH}_4^+$  and total phosphorous (TP) because of the longer contact time and increased adsorption capacity. The removal of  $\text{NH}_4^+$  and OM is mainly attributed to adsorption and biodegradation. The increase of TP and  $\text{NO}_3^-$  concentration mainly results from discharge and nitrification in riverbed soils, respectively. This study underscores the role of low-permeability layers as barriers in groundwater protection. Neglect of fingers or preferential flow may cause underestimation of pollution risk.

**Keywords** Laboratory experiments/measurements · Solute transport · Soil columns · Seepage control · Mobile-immobile model

## Introduction

Reclaimed water from municipal sewage is widely used for agricultural, industrial and ecological purposes. (Levine and Asano 2004; Meneses et al. 2010). When it is added to rivers to augment river flow, the main concern is riverbed leakage and the potential to contaminate groundwater. A specific example of such a case is the River Yongding in Beijing, China. Due to upstream withdrawals, this river dries up before reaching Beijing. Treated wastewater is discharged into the dry riverbed. Because several abstraction plants pump groundwater nearby, there is the potential that the reclaimed water may infiltrate and put groundwater at risk. For this reason, a barrier layer was added to the riverbed in 2010.

Sand-bentonite or silt-bentonite mixtures are commonly utilized as liner materials because they reduce permeability and serve as reactive barriers (Alther 2004; Amadi and Eberemu 2013; Mollins et al. 1996). Similar to a canal liner (Yao et al. 2012), a bentonite/silt mixture was installed as a layer on the River Yongding riverbed to inhibit seepage. This layer supplemented the existing low-permeability soil layer, which also prevents reclaimed water from discharging directly into groundwater. The joint performance of an artificial liner and a riverbed's existing low-permeability soil layer, in reducing seepage and controlling the fate of the various contaminants in the reclaimed water, has yet to be investigated.

The artificial liner is usually thin, with a permeability that is significantly lower than that of the underlying vadose zone. Layered media can differ significantly from homogeneous media where infiltration is concerned. For example, the underlying (more permeable) layer will remain unsaturated due to the overlying low-permeability layer. The top layer controls the infiltration rate, which reaches a constant value. Water movement through the lower, more permeable layer is non-uniform. Indeed, the wetting front tends to be unstable and can form narrow wetting columns or “fingers” (Hill and Parlange 1972; Hillel and Baker 1988).

Received: 26 March 2014 / Accepted: 27 August 2014  
Published online: 23 September 2014

© Springer-Verlag Berlin Heidelberg 2014

H. Hu · X. Mao (✉) · C. Liu · P. Li  
Center for Agricultural Water Research in China,  
China Agricultural University, Beijing, 100083, China  
e-mail: maoxiaomin@cau.edu.cn  
Tel.: +86-10-62738498

D. A. Barry  
Laboratoire de technologie écologique, Institut d'ingénierie de  
l'environnement, Faculté de l'environnement naturel, architectural  
et construit (ENAC),  
Ecole polytechnique fédérale de Lausanne (EPFL), Station 2, 1015,  
Lausanne, Switzerland

Reclaimed water often contains nitrogen, phosphorus and various types of organic matter (OM), which may pose a threat to groundwater.  $\text{NH}_4^+$  (ammonium) is a common and unstable form of nitrogen in reclaimed water. It can be adsorbed by the soil, or converted to  $\text{NO}_3^-$  (nitrate) by nitrification (Heatwole and McCray 2007; Jellali et al. 2010; Saâdi and Maslouhi 2003; Starr et al. 1974). Phosphate-related reactions are highly variable and depend on the soil type (McCray et al. 2000). The phosphate can either be removed from the water by sorption and precipitation (especially in the presence of heavy metals, Panasiuk 2010), or released into the water when background concentrations are high (Lin and Banin 2005; Shariatmadari et al. 2006). The amount of OM is quantified by chemical/biochemical oxygen demand (COD/BOD). OM is commonly biodegraded under aerobic or anaerobic conditions, and is accompanied by transformation of other species (Essandoh et al. 2011). Several kinetic models have been developed to describe the aforementioned reactions. First-order kinetic models are the most widely used due to their simplicity (Yamaguchi et al. 1996), while Monod-type models are more comprehensive (MacQuarrie and Sudicky 2001), although at the cost of more parameters.

In order to assess the risk of reclaimed water or wastewater use for aquifer recharge or soil aquifer treatment (SAT) and other purposes, soil column tests are widely carried out. Güngör and Ünlü (2005) examined the removal efficiencies of nitrite and nitrate in 88-cm-long soil columns ponded with 2.5 cm of wastewater. Jellali et al. (2010) conducted soil column experiments in 1-m-long saturated columns to test the transport process of  $\text{NH}_4^+$  in wastewater. Essandoh et al. (2011) used a 2-m-long saturated laboratory soil column to assess the removal of typical pollutants in artificial wastewater. A larger-scale leaching test was conducted by Ollivier et al. (2013) in a steel cylinder (3 m diameter and 4.5 m long) to analyze geochemical processes associated with treated water inflow; however, no studies cover both preferential flow induced by a layered soil structure and biogeochemical reactions occurring during leaching of reclaimed water.

The main aim of this study was to carry out large-column experiments on reclaimed water seepage through two-layered media, where the upper layer's permeability was much lower than that of the lower layer. The results were analyzed with the aid of a multi-species reactive transport model, which considered the fate and transport of  $\text{NH}_4^+$ ,  $\text{NO}_3^-$ , total phosphorous (TP) and OM. These investigations permit evaluation of the performance of bentonite mixtures, which are used as low-permeability layers for control of pollutants.

## Materials and methods

### Column experiment design

The large soil column experiments were designed to investigate the reactive transport of reclaimed water

through a vadose zone covered by different low-permeability layers. The experiments were carried out in four transparent acrylic columns, each 300-cm-long with an internal diameter of 49 cm. The columns were filled to a height of 200 cm with soil excavated from the bed of the River Yongding (Mentougou district of Beijing). When filling the soil columns, a 25-cm-thick layer of washed gravel was placed at the bottom of each column as the inverted filter. Then, the excavated soils were fully mixed and sieved through a 2-cm screen and packed into the column in 30-cm increments with an initial mass water content,  $\omega_0$ , of 4 % and bulk density  $\rho$  of  $2.1 \text{ g cm}^{-3}$ . The high bulk density is probably due to the high proportion of sand (92.9 %, see Table 1) in the riverbed, which has a large particle density. The surface of each layer was roughened between each soil addition to better approximate the field condition. After the low-permeability layer was added to the soil (if applied), a final 5.5-cm-thick layer of washed gravel was added to protect the soil layer from flushing. A Mariott bottle was used to supply reclaimed water while maintaining 30 cm of constant ponding head. The reclaimed water was collected from one of the Beijing wastewater treatment plants considered for supplementing the River Yongding. All experiments were conducted with flow oriented downwards. Ten soil-water collectors were installed every 20 cm along the soil column to collect solution by vacuum pumps. A schematic diagram of experimental setup is shown in Fig. 1.

In order to compare the performance of low-permeability layers with different bentonite ratios (by weight), small-column experiments were conducted to test the relationship between the hydraulic conductivity ( $K$ ) and the proportion of bentonite in the low-permeability layers. The bulk density of the small soil column was  $1.27 \text{ g cm}^{-3}$ . The results are shown in Fig. 2.

Then, a 2-cm-thick low permeability layer was added to three of the large-column (300 cm) set-ups. This added layer consisted of a compacted mixture of silt loam and bentonite, with a bentonite content of 12 % (named BE12 hereafter), 16 % (BE16) and 19 % (BE19) to represent high-, medium- and low-permeability layers, respectively. One column, without a covering layer, served as a blank control (named BC hereafter).

The three columns (BE12, BE16 and BE19) were leached with reclaimed water obtained from the water recycling plant. The leachate from the outlet at the bottom of the columns was collected. Concentrations of the four target pollutants in leachate were monitored, i.e.,  $\text{NH}_4^+$ ,  $\text{NO}_3^-$ , TP and OM. Column BC was leached with freshwater initially. After about 6 h, steady-state flow was achieved, at which time sodium chloride solution ( $20 \text{ g L}^{-1}$ ) was injected into column BC as a tracer. The whole experiment lasted from 26 August 2010 to 11 November 2011. Because the columns were apparently clogged after 210 d, only the experimental results in the first 210 days were analyzed.

The main physical and chemical properties of the soil are listed in Tables 1, 2 and 3.

**Table 1** Particle size distribution (%) of soils used in the study

	Coarse sand (2–0.5 mm)	Medium sand (0.5–0.25 mm)	Fine sand (0.25–0.05 mm)	Silt (0.05–0.005 mm)	Clay (<0.005 mm)
Riverbed soil	8.6	37.3	47	7.1 (for total silt and clay)	
Silt loam	-	2.5	10.5	63	24
Bentonite	0.48	2.6	33.92	38	25

### Multi-species reactive transport model

#### Transport equations

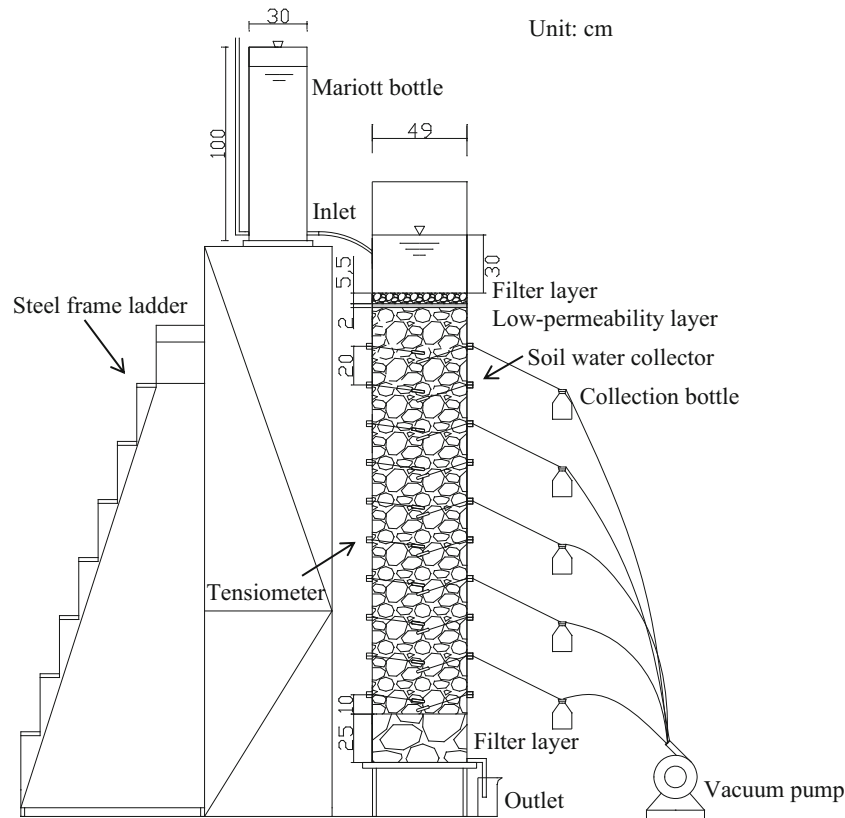
Columns BE12, BE16 and BE19 were characterized by distinctly layered soil structures, with a thin fine-textured (low  $K$ ) layer and a thick coarse-textured underlying layer (high  $K$ ). As demonstrated previously (Hill and Parlange 1972; Hillel and Baker 1988), when the wetting front reaches the interface, the infiltration rate is near-constant. The upper layer stays saturated while the lower layer is divided into two (immobile and mobile) zones, with narrow wetting columns or “fingers” as shown in Fig. 3. In the study, it took less than 1 d for the top low-permeability layer to become fully saturated, which for this layer means the unsaturated transport period is short compared with the saturated transport period (210 days). Thus, the initial unsaturated period was ignored. For the second layer, preferential flow and associated reactions are important factors in transport. The behavior depicted in Fig. 3 is a simplified outline of the mechanisms involved in fingering. These are thoroughly discussed in the recent review of DiCarlo (2013). Despite its simplifications, the

behavior described in Fig. 3 is an acceptable idealization for the purpose of the study, which is to recognize that fingers are likely in the circumstances under investigation, and that the consequences of these fingers on solute transport need to be accounted for in the modelling approach.

Transport in the upper, saturated layer can be described by classical advection–dispersion equation (ADE; e.g., Spiteri et al. 2007),

$$\frac{\partial C^j}{\partial t} = D_L \frac{\partial^2 C^j}{\partial z^2} - v_0 \frac{\partial C^j}{\partial z} + r^j \quad (1)$$

where the superscript  $j$  refers to species  $j$  ( $j=1, 2, 3, \dots$ ),  $C^j$  is the concentration of species  $j$  ( $\text{mg L}^{-1}$ ),  $t$  is time (s),  $z$  is distance (m),  $v_0$  is the average pore-water velocity ( $\text{m s}^{-1}$ ),  $D_L$  is the hydrodynamic dispersion coefficient ( $\text{m}^2 \text{s}^{-1}$ ),  $D_L = D_e + \alpha_L v_0$ ,  $D_e$  is the effective diffusion coefficient ( $\text{m}^2 \text{s}^{-1}$ ),  $\alpha_L$  is the longitudinal dispersivity (m), and  $r^j$  is the source/sink term for species  $j$  ( $\text{mg L}^{-1} \text{s}^{-1}$ ).

**Fig. 1** Schematic diagram of the large-column experimental setup

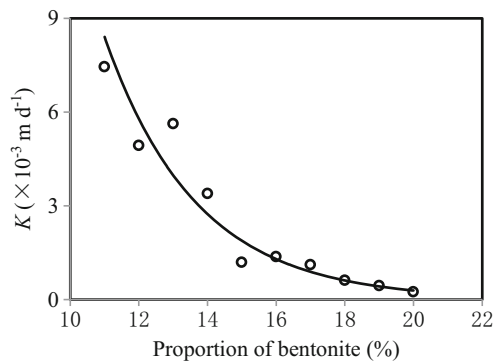


**Fig. 2** Relationship between hydraulic conductivity  $K$  and proportion of bentonite in silt loam

Since the soils were well mixed and sieved through the same screen before being packed into the columns, the column BC (without the low-permeability layer) can be considered as a uniform soil column in which one-dimensional (1D) advective–dispersive transport occurs; thus, Eq. (1) is also applicable for case BC to simulate the breakthrough of chloride ( $\text{Cl}^-$ ).

For the case where fingering is present, the flow is no longer 1D, and solute transport will no longer be adequately modeled using Eq. (1). Previously, it was shown that in this case the mobile–immobile region model (MIM, Coats and Smith 1964) can reasonably describe the solute transport (Griffioen and Barry 1999). Because the experiments reported here were not designed to capture details of fingered flow, application of the MIM is essentially phenomenological, although this point is briefly elaborated on later in the “Discussion” section. In a 1D steady flow system, the multi-species MIM (Smedt and Wierenga 1979) with reaction (in the mobile zone) is given by:

$$\theta_m \frac{\partial C_m^j}{\partial t} + \theta_{im} \frac{\partial C_{im}^j}{\partial t} = \theta_m D_{mL} \frac{\partial^2 C_m^j}{\partial z^2} - v_m \theta_m \frac{\partial C_m^j}{\partial z} + r_m^j \quad (2)$$

$$\theta_{im} \frac{\partial C_{im}^j}{\partial t} = \alpha (C_m^j - C_{im}^j) \quad (3)$$

where the subscripts m and im refer to mobile and immobile water, respectively, and  $\theta_m$  and  $\theta_{im}$  are the water-filled porosity ( $\text{cm}^3 \text{cm}^{-3}$ , fraction of total volume) in each region.  $C_m^j$  and  $C_{im}^j$  are, respectively, the concentrations of species  $j$  in the mobile and immobile regions ( $\text{mg L}^{-1}$ ),  $v_m$  is the average pore-water velocity in

the mobile zone ( $\text{m s}^{-1}$ ),  $D_{mL}$  is the hydrodynamic dispersion coefficient in mobile zone ( $\text{m}^2 \text{s}^{-1}$ ),  $D_{mL} = D_e + \alpha_{mL} v_m$ ,  $\alpha_{mL}$  is the longitudinal dispersivity in the mobile zone (m),  $r_m^j$  is the source/sink term of species  $j$  in the sublayer ( $\text{mg L}^{-1} \text{s}^{-1}$ ) and  $\alpha$  is the first-order mass transfer coefficient ( $\text{s}^{-1}$ ). If the mobile–immobile concept is applied to the layer in which fingering occurs, then the MIM moisture contents can be estimated based on the total volume of water in the fingers, and in the bypassed region, as proportions of the total volume in this layer.

Flux of all chemical species is conserved across the interface of the two layers (Barry and Parker 1987; Zhou and Selim 2001):

$$\left( q C_{\text{top}} - \theta_{\text{top}} D_{\text{top}} \frac{\partial C_{\text{top}}}{\partial z} \right) \Big|_{z \rightarrow L_1^-} = \left( q C_{\text{sub}} - \theta_{\text{sub}} D_{\text{sub}} \frac{\partial C_{\text{sub}}}{\partial z} \right) \Big|_{z \rightarrow L_1^+} \quad (4)$$

The subscripts top and sub signify the top layer and sublayer, respectively, and  $L_1$  is the position of the interface between the two layers. PHREEQC-2 (Parkhurst and Appelo 1999), which implements the aforementioned equations, was applied to simulate multi-species reactive transport in the experiments.

*Source/sink term and related reactions: reactions in the low-permeability layer (mixture of sodium bentonite and silt loam)*

The reactions of target solutes were considered separately in both the layers, considering the different soil characteristics and redox conditions in each. Silt loam and bentonite (in the low-permeability layer) strongly adsorb  $\text{NH}_4^+$  (Buragohain et al. 2013; Cameron and Klute 1977). The adsorption was quantified using batch adsorption experiments.

Kinetic adsorption of  $\text{NH}_4^+$  is shown in Fig. 4a. The time required to achieve equilibrium for  $\text{NH}_4^+$  (about 6 h) in both cases is longer than the travel time through the top layer (1–2.4 h in BE12 and 3.3–4.8 h in BE19, calculated by  $L_{\text{top}}/v_{\text{top}}$ , where  $L_{\text{top}}$  is the thickness of top layer,  $v_{\text{top}}$  is the pore-water velocity in the top layer). Thus, in the transport model, adsorption was described by first-order kinetics:

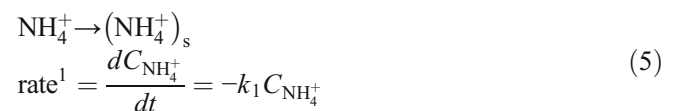


**Table 2** Saturated hydraulic conductivity values for soils used in the study

	Riverbed soils	Low-permeability soils		
		BE12	BE16	BE19
Saturated hydraulic conductivity $K$ ( $\text{m d}^{-1}$ ) <sup>a</sup>	8.6	$4.93 \times 10^{-3}$	$1.37 \times 10^{-3}$	$4.43 \times 10^{-4}$

<sup>a</sup>The saturated hydraulic conductivity of riverbed soils was estimated by Darcy’s law in column BC. The value of  $K$  of low-permeability soils was estimated by Darcy’s test in the small columns



**Table 3** Background concentrations in riverbed soil

Parameter	Value (mg kg <sup>-1</sup> )
Total phosphorus (TP)	340
Nitrate (NO <sub>3</sub> <sup>-</sup> )	3.46
Ammonium (NH <sub>4</sub> <sup>+</sup> )	<1.25
Organic matter (OM)	720

where  $k_1$  is the first-order rate constant (s<sup>-1</sup>) for NH<sub>4</sub><sup>+</sup> adsorption. The subscript *s* means the species in the adsorbed state.

For TP, two reactions normally occur in the water–soil system, i.e., adsorption and precipitation (McCray et al. 2000). Given the small ratio of sodium bentonite, precipitation/dissolution of phosphate minerals is not the main removal (from the liquid phase) process in the layer. The adsorption kinetics in Fig. 4 indicates a relatively long time to reach equilibrium (about 12 h in all the BE cases) compared with the travel time in the top layer; hence, the adsorption equilibrium may not be achieved in this layer. As in the previous, TP adsorption was described by first-order kinetics:

$$\text{TP} \rightarrow (\text{TP})_s \quad \text{rate}^2 = \frac{dC_{\text{TP}}}{dt} = -k_2 C_{\text{TP}} \quad (6)$$

where  $k_2$  is the first-order rate constant (s<sup>-1</sup>) for TP adsorption.

Reactions of OM and NO<sub>3</sub><sup>-</sup> were not considered in the top layer given the short travel time (4.8 h for BE19), which may not allow biochemical degradation to occur (Schmidt et al. 2011). Additionally, the travel time in the bottom layer (2 d for BE19) is longer than in the top layer, so transformations such as nitrification in the bottom layer are much greater there than in the top layer.

*Source/sink term and related reactions: reactions in riverbed soil*

The large amount of accumulated phosphate (340 mg kg<sup>-1</sup>, Table 3) in riverbed soil leads to P release by desorption and organic matter degradation (Sharpley et al. 1981; Surridge et al. 2007). The release process (Shariatmadari et al. 2006) was described by:

$$(\text{TP})_s \rightarrow \text{TP} \quad \text{rate}^3 = \frac{dC_{\text{TP}}}{dt} = k_3 C_{\text{TP}} \quad (7)$$

where  $k_3$  is the first-rate constant (s<sup>-1</sup>) of TP release.

OM degradation in the sublayer was modeled by first-order kinetics (Tchobanoglous et al. 2003):

$$\text{OM} \rightarrow \text{IOM} \quad \text{rate}^4 = \frac{dC_{\text{OM}}}{dt} = -k_4 C_{\text{OM}} \quad (8)$$

where IOM is inorganic matter produced from biodegradation and  $k_4$  is the first-order degradation rate constant (s<sup>-1</sup>) for OM.

In the underlying layer, both adsorption and nitrification may contribute to the reduction of the amount of ammonium. The two processes (Cameron and Klute 1977; Yamaguchi et al. 1996) were included in the model and described, respectively, by:

$$\text{NH}_4^+ \rightarrow (\text{NH}_4^+)_s \quad \text{rate}^5 = \frac{dC_{\text{NH}_4^+}}{dt} = -k_5 C_{\text{NH}_4^+} \quad (9)$$

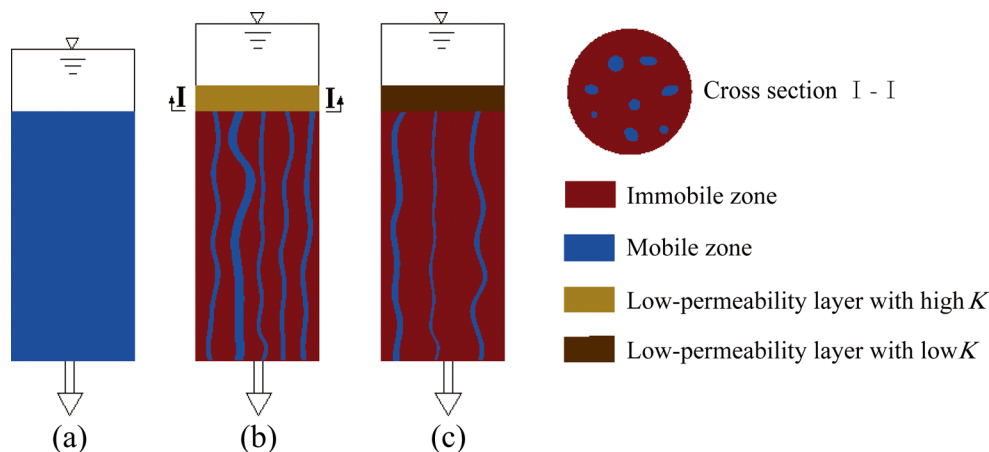


**Fig. 3** Conceptual motivation for using the mobile–immobile region model. Flow patterns under ponding with **a** no low-permeability layer, **b** low-permeability layer with relatively high  $K$  and **c** low-permeability layer with relatively low  $K$ . The flux through the column is controlled by the permeability of the upper layer, whereas the finger width (and thus the flux through each finger, since the core of each finger is near-saturated) is controlled by the lower layer. Hence, the number of fingers varies with the permeability of the upper layer (Hill and Parlange 1972; Parlange and Hill 1976; Selker et al. 1992)

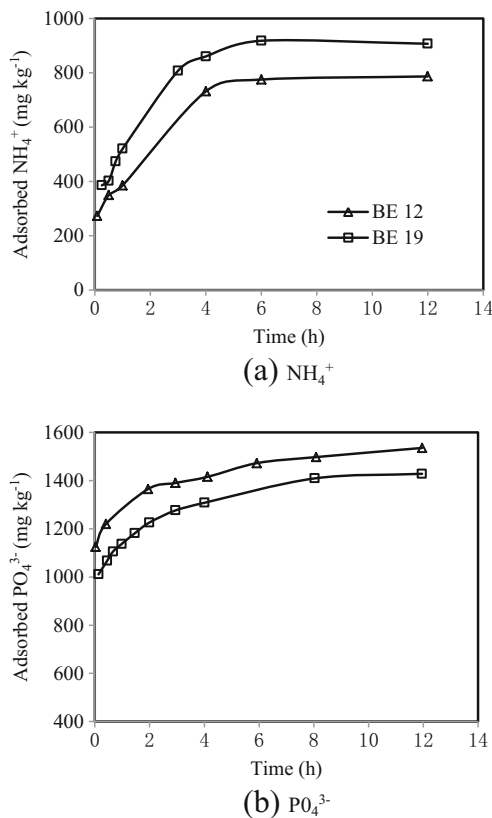
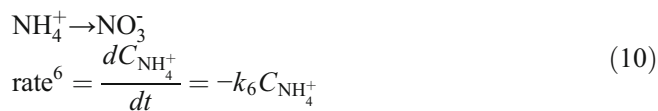
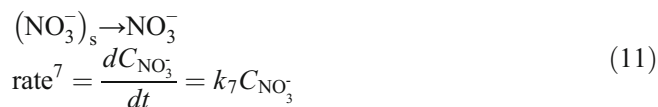


**Fig. 4** Kinetic adsorption of **a**  $\text{NH}_4^+$  and **b**  $\text{PO}_4^{3-}$  in the top-layer soil of BE12 and BE19, as measured in batch experiments



where  $k_5$  is the first-order adsorption rate constant ( $\text{s}^{-1}$ ) and  $k_6$  is the first-order nitrification rate constant ( $\text{s}^{-1}$ ) in the sublayer.

$\text{NO}_3^-$  has a background concentration of  $3.46 \text{ mg kg}^{-1}$  (Table 3) in the riverbed soil.  $\text{NO}_3^-$  discharge was simulated using first-order kinetics (Ling and El-Kadi 1998):



where  $k_7$  is the first-order discharge rate constant ( $\text{s}^{-1}$ ) of  $\text{NO}_3^-$ .

Denitrification was not included in the model, since no sign of denitrification was found, as suggested by the small increase of  $\text{NO}_3^-$  concentration in the outflow (see “ $\text{NO}_3^-$ ” section).

## Parameter determination

### Transport parameters in case BC

The averaged pore-water velocity  $v_0$  and dispersivity  $\alpha_L$  were obtained by fitting the breakthrough curve (BTC) to the observed data in case BC, considered as a homogeneous soil column, an assumption that is supported by the fit (calculated using PHREEQC-2) of the  $\text{Cl}^-$  BTC (Fig. 5). Boundary conditions used for the fit were a constant concentration of  $19.3 \text{ g L}^{-1}$  at the column entrance, and a zero-gradient condition at the exit. The initial concentration was set as  $0.26 \text{ g L}^{-1}$  throughout the column. The calibrated parameters used were the averaged pore-water velocity,  $v_0$ , which was  $1.45 \text{ cm min}^{-1}$  and the dispersivity,  $\alpha_L$ , estimated as  $0.08 \text{ m}$ . Consequently, the saturated water content  $\theta_{s\text{-BC}}$  was obtained from the Darcy velocity divided by the pore-water velocity in this case, i.e.,  $\theta_{s\text{-BC}} = q_0/v_0$  (the observed  $q_0 = 0.27 \text{ cm min}^{-1}$ ), about  $0.2 \text{ cm}^3 \text{ cm}^{-3}$ . The diffusion coefficient (typical value around  $10^{-9} \text{ m}^2 \text{ s}^{-1}$ ) was ignored as it was negligible compared with dispersion ( $\alpha_L v_0 = 2 \times 10^{-5} \text{ m}^2 \text{ s}^{-1}$ ).

### Transport parameters in cases BE

The infiltration rate or Darcy velocity in the column with the low-permeability layer (case BE) was calculated based on:

$$Q = q_{\text{top}}A = q_{\text{bot}}A \quad (12)$$

where  $Q$  is volumetric flow rate ( $\text{m}^3 \text{ s}^{-1}$ ),  $A$  is the cross-section area of the column ( $\text{m}^2$ ),  $q_{\text{top}}$  and  $q_{\text{bot}}$  are the Darcy velocity ( $\text{m s}^{-1}$ ) through top and bottom layers, respectively.

The area wetted by the fingers  $\beta_m = \theta_m/\theta_{s\text{-bot}}$  ( $\theta_{s\text{-bot}}$  is the saturated water content in the sublayer,  $\text{cm}^3 \text{ cm}^{-3}$ ) in the sublayer for cases BE12, BE16 and BE19 was determined from measured data using:

$$V_0(\theta_{s\text{-bot}} - \theta_0)\beta_m = V_m \quad (13)$$

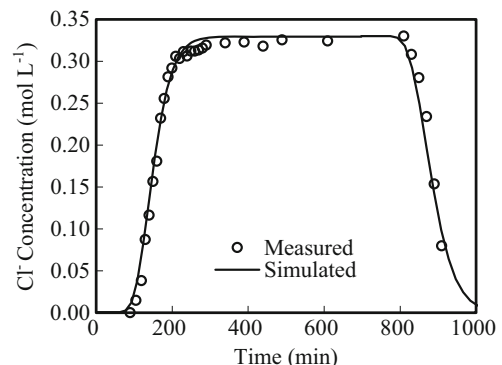


**Fig. 5** Comparison of measured and simulated effluent concentrations of  $\text{Cl}^-$  for case BL (homogeneous soil)

where  $V_0$  is the volume of sublayer ( $\text{cm}^3$ ), and  $(\theta_{s\text{-bot}} - \theta_0)$  is the water content increase in sublayer during the leaching process,  $\theta_0$  is the initial water content on a volume basis.  $\theta_{s\text{-bot}}$  was assumed to be the same for all three BE columns and was set to the same value ( $\theta_{s\text{-BC}}$ ) as the BC column (because they were filled with soil with the same texture and density).  $V_m$  is the water volume of the fingers in the sublayer ( $\text{cm}^3$ ), estimated as the amount of water inflow from the start of the experiment until the outflow at the bottom of the column was detected less the water volume in the saturated top layer. The calculated values of  $\beta_m$  (Table 4) are within the range of reported values (Griffioen et al. 1998). As expected,  $\beta_m$  decreases as the permeability of the upper layer decreases (Fig. 3, low  $K$ ), since fewer fingers are formed then.

The velocity of the fingers in the sublayer was calculated using  $v_m = q_{\text{bot}}/\theta_m$ . According to the experimental results for cases BE12, BE16 and BE19,  $v_m$  underwent two evidently stable phases, with a first high-velocity stage from days 1–40 of the experiment, and a second low-velocity stage from days 41–210. It is suggested that the second stage was due to soil pore clogging. Correspondingly, two stages of velocity were divided in the simulation as shown in Table 4.

Mass transfer coefficient  $\alpha$  should increase with the increase of  $v_m$ , because higher  $v_m$  can enhance the mixing in the mobile phase, and shorten the diffusion path length (Kamra et al. 2001; Li et al. 1994; Smedt and Wierenga 1984). The empirical relation (Maraqa 2001) between  $\alpha$  and  $v_m$  used in this study was

$$\alpha = 0.00076v_m^{0.76} \quad (14)$$

In summary, the transport parameters applied in the model are listed in Table 5.

#### Reaction rate coefficient

Determining how the two layers work together in controlling the transport and fate of contaminants is the main goal of this study, rather than the detailed investigation of reaction mechanisms and each reaction parameter. The adsorption rate constants for both  $\text{NH}_4^+$  and TP in the top layers were obtained from batch tests and fitting with column experiment results. The rate constant used for TP in the model is a little higher than that obtained from the batch adsorption experiment because precipitation may

also lead to a TP concentration decrease in the column experiments. The input parameter values are listed in Table 6.

The rate constants in the bottom layers were obtained by fitting the observed concentrations with guidance from literature values. The rate constants for nitrification used in the present study are an order of magnitude higher than the values reported by Starr et al. (1974). This difference is reasonable because the pore velocities reported by Starr et al. are nearly 10 times lower than those in the second stage of this study, and the  $\text{NH}_4^+$  concentrations are more than 10 times higher than the current values. The first-order rate constants for OM degradation used in the model are of the same order of magnitude as reported values.

Most rate constants for the second stage are lower than those for the first stage, which corresponds to the results of related studies, that rate coefficients are positively correlated with pore-water velocity (Brusseau 1992; Gaber et al. 1995; Guo et al. 1997; Pang et al. 2002).

#### Input concentration

The inflow concentration was measured by taking water samples from the water tank that stored reclaimed water to recharge the Mariott bottle (Fig. 1), and so is not the exact concentration of reclaimed water flowing from the Mariott bottles into the soil columns. The measured data can only reflect an approximation of the inflow concentration, so the approximate average value of measured data during the typical periods was applied as the input concentration for the simulation in each stage. The water tank was filled with reclaimed water three times during the experiment. The inflow concentration of  $\text{NO}_3^-$  exhibits a three-stage trend, while the other three solutes show approximately two stages (Fig. 6). The dividing points between two stages correspond to the time for refilling the water tank. The first stage of input concentrations is from 0 to 40 days, coinciding with that of the stage one velocity, described in the previous. The stages of input concentration were also marked in the following results.

#### Model performance criteria

The simulated values were compared with the measured values using the normalized root mean square error (NRMSE) and the index of agreement ( $d$ ) to evaluate the

**Table 4** Flow parameters related to mobile-immobile model

Experiment	Pore-water velocity ( $\text{cm d}^{-1}$ )				Mobile water fraction $\beta_m$	Transfer coefficient $\alpha$ ( $\text{d}^{-1}$ )	
	Days 1–40		Days 41–210			Days 1–40	Days 41–210
	Top	Bottom	Top	Bottom			
Case BE12	48.75	243.7	20	100	0.42	$1.22 \times 10^{-6}$	$6.24 \times 10^{-7}$
Case BE16	37.75	215.7	15.2	87.1	0.33	$1.12 \times 10^{-6}$	$5.62 \times 10^{-7}$
Case BE19	14.40	96	10	66.67	0.32	$6.05 \times 10^{-7}$	$4.59 \times 10^{-7}$

**Table 5** Determination of transport parameters

Parameter	Layer	Source
$q_0$	BC <sup>a</sup>	Obtained from experimental observations
$q_{top}$	Top	Obtained from experimental observations
$q_{bot}$	Bottom	Obtained from experimental observations
$v_0$	BC	Fitting Cl <sup>-</sup> BTC in case BC
$\theta_{s-BC}$	BC	$\theta_{s-bot} = \theta_{s-BC} = q_0/v_0$
$\theta_{s-bot}$	Bottom	$\theta_{s-bot} = \theta_{s-BC} = q_0/v_0$
$\alpha_L$	Bottom	Fitting the Cl <sup>-</sup> BTC in case BC, assumed constant in all cases
$\omega_0$	Bottom, BC	Measured before experiment
$\theta_0$	Bottom, BC	$\theta_0 = \omega_0 \rho$
$V_0$	Bottom	$V_0 = L \times \pi \times 24.5^2$ ( $L=200$ cm) <sup>b</sup>
$V_m$	Bottom	Observed in the experiment
$\theta_{s-top}$ <sup>c</sup>	Top	Assumed as 0.4 for cases BE12, BE16 and BE19
$v_{top}$	Top	$v_{top} = q_{top}/\theta_{s-top}$
$\theta_m$	Bottom	$\theta_m = \theta_{s-bot} \beta_m$
$v_m$	Bottom	$v_m = q_{bot}/\theta_m$
$C_m^j$	Bottom	$C_m^j _{z \rightarrow L_1} = C_m^j _{z \rightarrow L_1^+}$ (at the interface between two layers)

<sup>a</sup> BC refers to the layer of riverbed soils in case BC

<sup>b</sup>  $L$  is the length of the sublayer soil (cm)

<sup>c</sup>  $\theta_{s-top}$  is the saturated water content ( $\text{cm}^3 \text{cm}^{-3}$ ) in the top layer of BE12, BE16 and BE19, respectively

performance of the numerical simulation. These metrics are given by:

$$\text{NRMSE} = \frac{\sqrt{\frac{1}{N} \sum_{i=1}^N (O_i - S_i)^2}}{O} \quad (15)$$

where  $N$  is the total number of observations,  $i$  is the number of observed and simulated values,  $O_i$  are the observed values,  $S_i$  are the simulated values,  $O$  is the mean value of the observed data. A smaller NRMSE indicates better model accuracy. The  $d$  statistic is:

$$d = 1 - \frac{\sum_{i=1}^N (O_i - S_i)^2}{\sum_{i=1}^N (|O_i - O| + |S_i - S|)^2} \quad (16)$$

where  $S$  is the mean value of simulated data. The closer  $d$  is to 1, the more accurate the model.

## Results

### $\text{NH}_4^+$

As shown in Fig. 7, the relative concentration of  $\text{NH}_4^+$  in the effluent was usually below 0.1. The lowest relative concentration of  $\text{NH}_4^+$  (less than 0.01) was found in case BE19 for both measured and simulated results. Considering that the same sublayer soil was used, it was the liner materials that were mainly responsible for the different  $\text{NH}_4^+$  removal in these three cases. Higher proportion of bentonite in the low-permeability layer helps reduce the concentration of  $\text{NH}_4^+$  in the leachate. One reason is that more bentonite in the upper layer can adsorb more  $\text{NH}_4^+$  as shown in Fig. 4a. The other reason is that a higher proportion of bentonite in the upper layer decreases the pore-water velocity in both upper and bottom layers (Table 4) due to its swelling character (Mollins et al. 1996), which provides more time for  $\text{NH}_4^+$  to be exposed to the soil particles in the sublayer, so that nitrification occurs more completely. The simulation captures the behavior of the measured data except for some scattered data, i.e. the sharp rise in relative concentrations in BE12 and BE16 during the period from 89 to 135 days, which is possibly due to the preferential flow induced by macropores in the columns. Note that although the columns were repacked as evenly as possible, heterogeneity may still exist. It can be partly explained by the fact that the number of scattered data is more in cases BE12 and BE16 than in case BE19, while cases BE12 and BE16 show a higher flow rate than case BE19 (Table 4). According to Rosqvist et al. (2005), a high flow rate enhances preferential flow in soils with a heterogeneous structure. These scattered data were not captured by the numerical model; therefore, cases BE12 and BE16 show a relatively high value of NRMSE and low value of the index of agreement ( $d$ ) than case BE19 (Table 7).

### $\text{NO}_3^-$

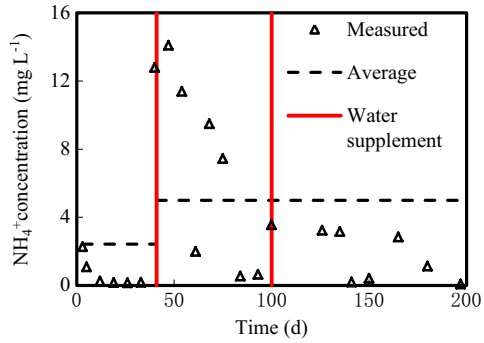
$\text{NO}_3^-$  concentrations behave similarly among the three cases. Measured and simulated outflow concentrations of

**Table 6** Reactions considered in the model and rate constants in each stage<sup>a</sup>

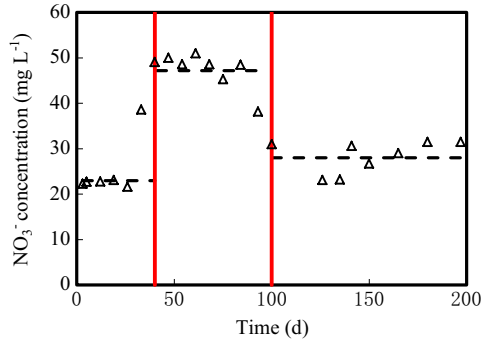
Layer	Reaction	$k$	Rate constant ( $\text{d}^{-1}$ )			Sources
			BE12	BE16	BE19	
Top	$\text{NH}_4^+$ adsorption	$k_1$	$7.08 \times 10^{-3}$	$8.33 \times 10^{-3}$	$9.17 \times 10^{-3}$	Fixed Measured
	TP adsorption	$k_2$	$1.17 \times 10^{-3}$	$1.29 \times 10^{-3}$	$1.416 \times 10^{-3}$	Fixed Measured
Bottom	TP release	$k_3$	1.7/0.65	1.7/0.6	0.75/0.42	Fit 6.00 (Li et al. 2012)
	OM degradation	$k_4$	1/0.4	1.2/0.4	0.6/0.35	Fit 0.09–0.52 (Hewitt et al. 1979)
	$\text{NH}_4^+$ adsorption	$k_5$	0.4/0.5	1.8/0.9	0.4/0.4	Fit Fitting with observed concentrations
	Nitrification	$k_6$	1.4/1	1.4/0.9	1.7/1.4	Fit 0.77 (Starr et al. 1974)
	$\text{NO}_3^-$ discharge	$k_7$	0.01/0.02/0	0.01/0/0	0.1/0.02/0.01	Fit Fitting with observed concentrations

<sup>a</sup> The fitted rate constants in different stages are separated by “/”, and the stage division method is based on the variation trend of pore velocities and input concentrations (Fig. 5)

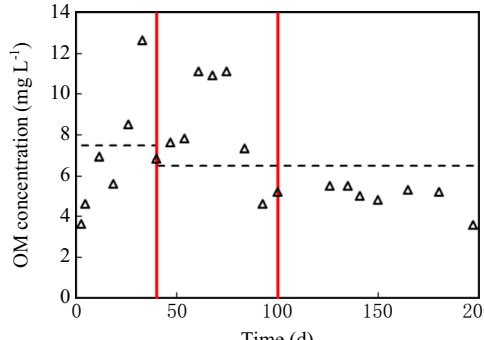




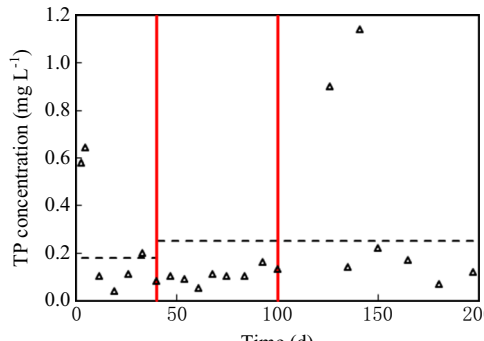
(a)  $\text{NH}_4^+$



(b)  $\text{NO}_3^-$

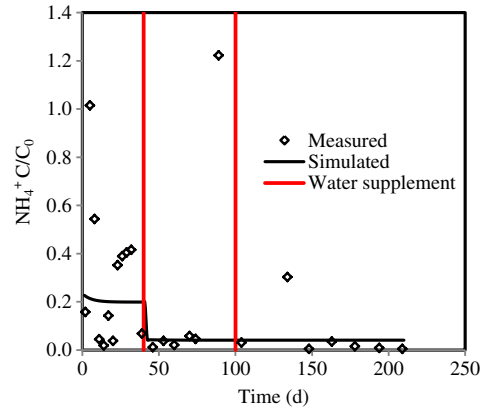


(c) OM

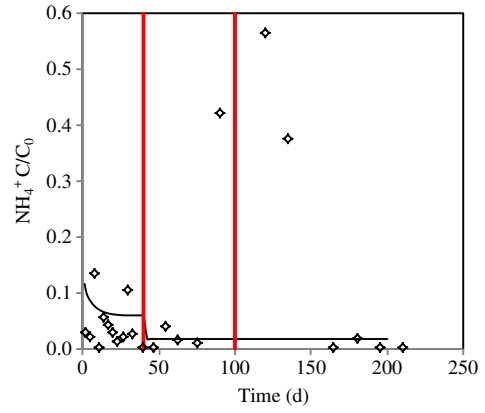


(d) TP

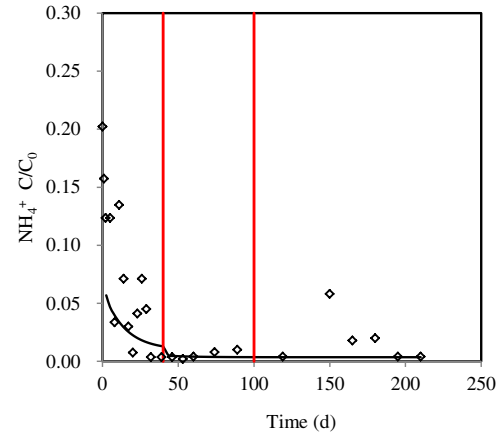
**Fig. 6** Measured inflow and model input concentrations of **a**  $\text{NH}_4^+$ , **b**  $\text{NO}_3^-$ , **c** OM, and **d** TP



(a) BE12



(b) BE16



(c) BE19

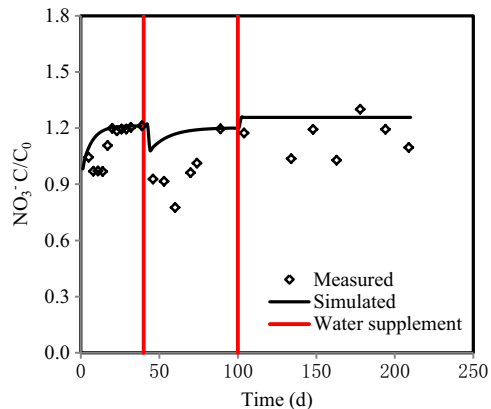
**Fig. 7** Measured and simulated concentrations of  $\text{NH}_4^+$  in cases **a** BE12, **b** BE16 and **c** BE19

$\text{NO}_3^-$  showed agreement, with the values of NRMSE between 0.14 and 0.24, though the index of agreement is low in cases BE12 and BE16 (Table 7). The heterogeneity in the columns mentioned in the preceding and reactions occurring in the water tank and Mariott bottles may contribute to the scatter of the measured data.

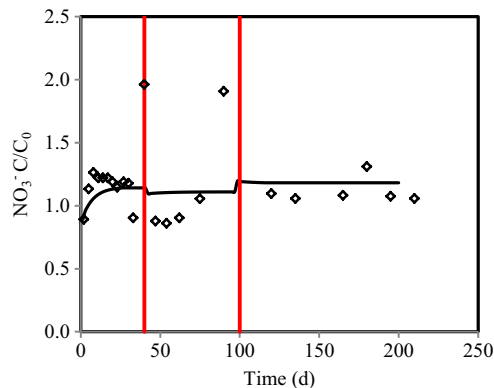
**Table 7** Statistical analysis of simulation results for solutes

	TP			NH <sub>4</sub> <sup>+</sup>			NO <sub>3</sub> <sup>-</sup>			OM		
	BE12	BE16	BE19	BE12	BE16	BE19	BE12	BE16	BE19	BE12	BE16	BE19
NRMSE	0.28	0.08	0.14	1.47	1.84	0.93	0.14	0.24	0.17	0.92	0.3	0.36
<i>d</i>	0.28	0.9	0.87	0.3	0.05	0.59	0.07	0.12	0.62	0.26	0.47	0.79

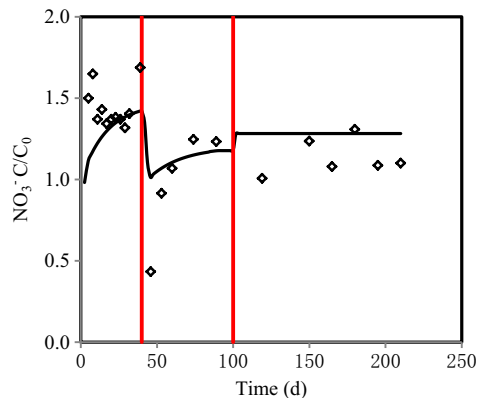
Most relative concentrations are higher than unity in Fig. 8. The increase of the outflow concentrations is caused by nitrification and discharge from the riverbed



(a) BE12



(b) BE16



(c) BE19

**Fig. 8** Measured and simulated concentrations of NO<sub>3</sub><sup>-</sup> in cases **a** BE12, **b** BE16 and **c** BE19

soil. The outflow concentration of NO<sub>3</sub><sup>-</sup> is influenced by the bentonite ratio in the low-permeability layer, with more bentonite in this layer, there is a higher concentration of NO<sub>3</sub><sup>-</sup> in the outflow. The relative concentrations in cases BE12 and BE16 are close to each other in the first stage, around 1.2, mainly because the two pore velocities are quite similar. The relative concentration in the first stage of case BE19 can increase to 1.4, which is higher than the other two cases, possibly because the higher percentage of bentonite helps reduce the pore-water velocity, and allows more time for complete reactions. The relative concentration of NO<sub>3</sub><sup>-</sup> (1.2) is almost the same among the three cases during the third stage (Fig. 8). This result indicates that the performance of the bentonite/silt-loam layer on NO<sub>3</sub><sup>-</sup> outflow concentration tends to be the same after leaching for 100 days. One reason is that the NO<sub>3</sub><sup>-</sup> stored in each soil column had been leached out at the late stage of the experiment, so the outflow concentration remained at a stable level. The other possible reason is that the supply of NH<sub>4</sub><sup>+</sup> for nitrification is limited in the later stage and leads to a limited production of NO<sub>3</sub><sup>-</sup>.

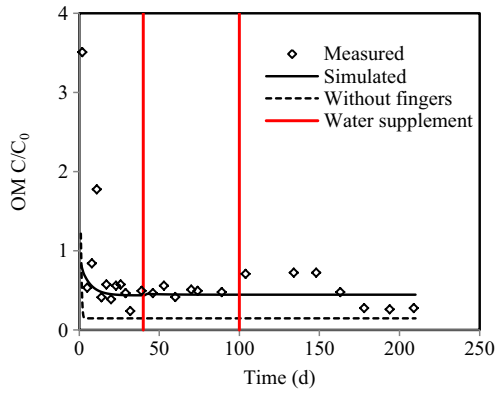
### OM

Figure 9 shows reasonable agreement between simulated and measured relative concentrations of OM. The relatively low values of NRMSE and high values of *d* are obtained in cases BE16 and BE19, indicating the accurate prediction of the model, while the fitness of the model in case BE12 is not as good as the other two cases (Table 7). A similar result is also found for TP. The main reason is the heterogeneity and fluctuations of the inflow concentration. The inflow concentration of case BE12 fluctuated more rapidly than the other two cases due to the more frequent filling of the Mariott bottle, which partly explains the high-frequency fluctuations in the outflow concentrations.

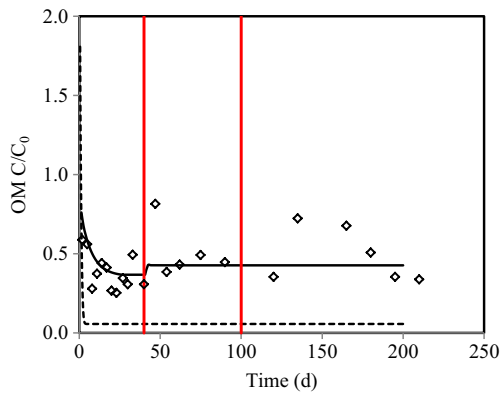
Good removal efficiency of OM is shown in the three cases. The outflow concentrations in the second stage are somewhat stable, with a relative concentration of 0.35 in case BE19, lower than that in case BE12 (about 0.5) and case BE16 (about 0.42). This comparison suggests that more bentonite in the low-permeability layer can help the degradation of OM. This is again because of the prolonged contact time in the case with more bentonite in the low-permeability layer; consequently, OM undergoes more degradation in the sublayer.

### TP

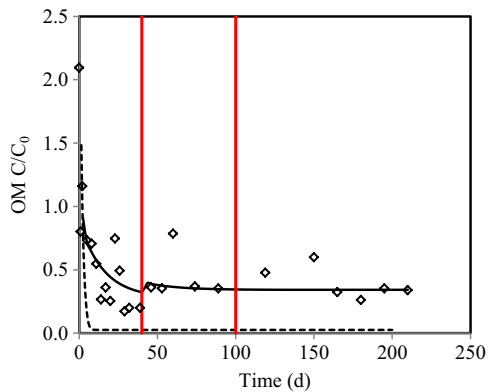
As shown in the experimental results (Fig. 10), most TP outflow concentrations in the three cases increased 3.5–5



(a) BE12



(b) BE16

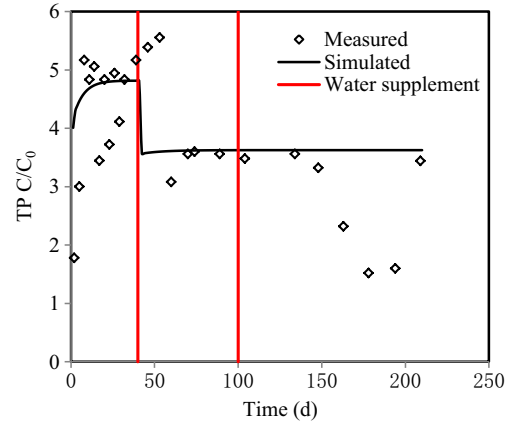


(c) BE19

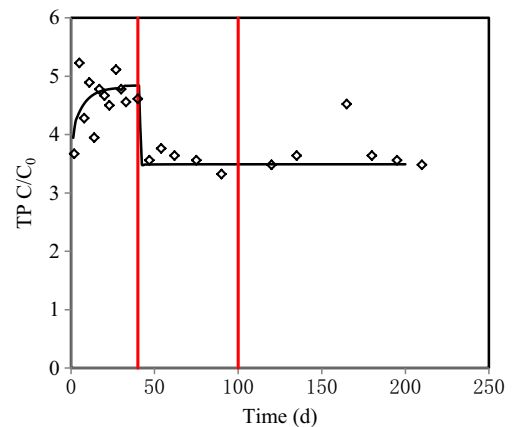
**Fig. 9** Measured and simulated concentrations of OM in cases **a** BE12, **b** BE16 and **c** BE19

orders compared with the inflow concentration. The high background concentration of the packed soil mainly contributes to the TP concentration increase. When the relatively low concentration of TP ( $0.2 \text{ mg L}^{-1}$ ) moved through the sublayer, a large amount of TP was flushed out.

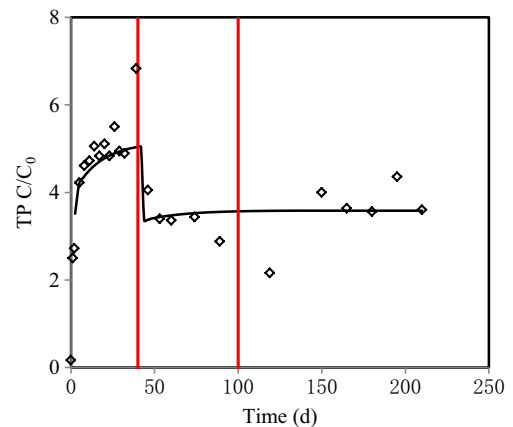
The outflow concentration can be roughly divided into two stages, with the relative concentration in the first stage higher than the second stage. The outflow TP concentration shows no clear difference among the three cases. Although more TP could be removed by adsorption with a



(a) BE12



(b) BE16



(c) BE19

**Fig. 10** Measured and simulated concentrations of TP in cases **a** BE12, **b** BE16 and **c** BE19

higher bentonite ratio in the top layer, the induced lower velocity in sublayer can lead to more TP release because of the prolonged residence time (Wassmann and Olli 2004). Therefore, the top layer and sublayer seem to play opposite roles in the outflow TP concentrations.

The simulation captured the behavior of TP concentrations, except the fluctuation of measured data before 50

d and after 150 d. The NRMSE values range between 0.08 and 0.28 (Table 7), while the values of index of agreement ( $d$ ) approach 1, except in case BE12, indicating that the accuracy of model is acceptable.

## Discussion

### Conservative transport with low permeability layers

To exclude the influence of reactions and to identify the effect of low-permeability layers on conservative solute transport, BTCs of  $\text{Cl}^-$  under the conditions of BE12, BE16 and BE19 were simulated. Figure 11 shows the BTC of BE19 obviously lags behind BE12 and BE16, because of the low pore-water velocity in case BE19. The BTC of BE19 is more spread than the other two cases. A higher bentonite ratio in the top layer increases the BTC asymmetry. One possible reason is that the increased bypassed water ratio (i.e., decreased  $\beta_m$ ) extends the time for  $\text{Cl}^-$  to achieve equilibrium between mobile and immobile zones. The other reason is that the lower exchange rate ( $\alpha$ ) in the case with a higher bentonite ratio increases the time to reach equilibrium between the two zones. The results suggest that bentonite addition in the top layer apparently increases physical nonequilibrium and the permeability of the top layer is negatively related to the physical nonequilibrium occurring in the sublayer.

The BTCs of BE12 and BE16 nearly overlap before 1 day (Fig. 11) due to the similar pore-water velocity and the same dispersivity, and diverge during the later stage. It is expected that the three BTCs will converge with sufficient elapsed time. Even if the outflow concentrations for the three conditions approach each other in the later period, the low permeability layer can still help reduce the  $\text{Cl}^-$  mass flux ( $CQ$ ) because these layers reduce the infiltration capacity of these soil systems. Previous studies (Cuthbert et al. 2010; Eguchi and Hasegawa 2008) indicated that preferential flow can increase the risk of contamination. The current study suggests that, in circumstances where physical nonequilibrium is evident, such as case BE19, solutes tend to store in the soil system. It should be noted that the preferential flow in Cuthbert et al.

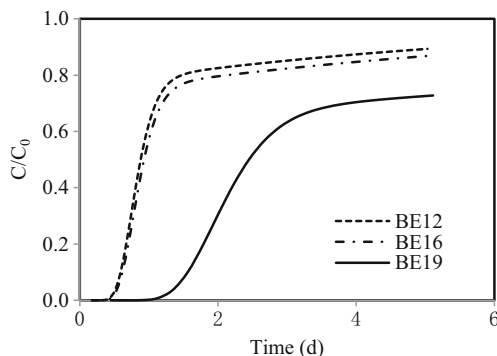


**Fig. 11** Simulated  $\text{Cl}^-$  concentration in cases BE12, BE16 and BE19

(2010) and Eguchi and Hasegawa (2008) is induced by fractures and macropores rather than stratification.

### Effect of fingers on pollutant transport

The mobile-immobile model for reactive solutes is designed to depict the experimental results with the low-permeability layer. To compare the effect of taking/neglecting the induced fingering, the ADE was applied to model the three experimental cases without considering fingers, i.e., uniform transport. The same inflow flux and reaction coefficients with experimental conditions were supplied. OM was chosen as an example to demonstrate the difference.

The BTCs of OM under the three treatments are shown in Fig. 9 (dashed lines). Less reduction is found with fingers in each condition. For a given volume of input reclaimed water, the fingered flow will induce deeper penetration of the soil since not all the pore space is used. Consequently, the shorter solute travel time for preferential flow [ $L/(q_{\text{bot}}/\theta_m)$ ] compared with uniform flow [ $L/(q_{\text{bot}}/\theta_{s-\text{bot}})$ ] (Table 8) results in fast transport of solutes through the column. Smaller pore-water velocities would enhance effluent quality because a longer residence time allows for a more complete reaction. For example, the travel time in BE12 is 0.8 d with fingers and 2.1 d without (Table 8). By using the same degradation constant  $1 \text{ d}^{-1}$  in both preferential and uniform flow conditions, it just takes 2.3 d for 90 % OM removal without considering fingers. By contrast, OM is degraded only 52 % during the whole experiment with fingers.

As the kinetic reaction coefficients were kept the same in the two flow conditions, the travel time mainly contributes to the different leachate concentrations. Singh et al. (2002) noted that infiltration into preferential flow pathways greatly reduces sorption due to a reduced contact area with soil and a reduced contact time. Similarly, less reduction of  $\text{NH}_4^+$  and OM was observed when considering fingers. The result also underscores that neglect of fingering could underestimate pollution risk for the soil system with a low-permeability layer overlying a high-permeability layer.

### Physical interpretation of mobile and immobile region behavior

In this study, the mobile-immobile model behavior is due to the fingers being a mobile region and the surrounding soil being an immobile region after the fingers were formed and kept stable. This assumption implies that the moisture content of the fingers and of the bypassed zone was constant and thus the advective velocity in each finger is constant. Nevertheless, it is likely that that varies between different fingers and within a single finger because of the soil heterogeneity and different soil moisture distribution. In the study of Griffioen and Barry (1999), the two-region model behavior is attributed to the different travel times in different fingers because soil moisture varies laterally and longitudinally (along and



**Table 8** Travel time (d) through the sublayer and removal efficiency (%) of OM under the preferential and uniform flow conditions

Travel time (d)	BE12	BE16	BE19	Removal efficiency (%)	BE 12	BE16	BE19
With fingers	0.8	0.9	2.1	With fingers	52	66.6	68
Without fingers	2.1	2.6	6.9	Without fingers	98	99.2	99.6

across a finger), though the mass exchange between fingers and surrounding soils was neglected. It is suggested that the possible mechanism of solute transport along fingers includes both the interaction of the mobile fingers and the immobile regions around the fingers and the velocity variation in different fingers.

## Conclusions

Installing a low-permeability layer onto the vadose zone creates a distinctly layered soil structure. The infiltration processes and the induced transport behavior in the created structure differ significantly from the single layer of riverbed soils without a barrier. Fingering flow results from the layered soil structure, i.e., the thin, low-permeability layer overlying a coarse (highly permeable) layer. Based on the monitored results from a set of large-scale soil column experiments with reclaimed water leaching through three kinds of low-permeability layers and underneath the vadose zone, a mobile-immobile model with multi-species reactions was established.

Results suggest that the higher amount of bentonite in the low-permeability layer, the more effective it was in removing OM and  $\text{NH}_4^+$ , mainly because of reactions that occurred in the fine textured layer and reduced pore-water velocity in the soil system. The low-permeability layers help release the background TP and  $\text{NO}_3^-$  from the soil during the experiment, but the performance of the low-permeability layers on these two species needs long-term observation. Neglect of fingering would underestimate the pollution risk under the soil system with a low-permeability layer overlying a high-permeability layer.

A modeling method is provided in the paper for evaluating pollutants leaching in a distinctly layered soil system such as a vadose zone with low-permeability treatment, soil-aquifer treatment system, or solid-waste landfill site, etc. To further evaluate the model, well-controlled column experiments and field studies should be carried out with more detailed monitoring on the flow behavior, the species transport and their reaction products, as well as more detailed investigation of the soil microorganisms and their behavior.

**Acknowledgements** This study was funded by Projects of National Natural Science Foundation of China (Grant No. 51379207), Innovation Fund for Graduate Student of China Agricultural University (Grant No. KYCX2011087) and Beijing Municipal Science and Technology Project (Grant No. D090409004009004). The authors would like to thank the editor Elizabeth Screation, the associate editor and anonymous reviewers for their detailed and thorough reviews.

## References

- Alther G (2004) Some practical observations on the use of bentonite. *Environ Eng Geosci* 10(4):347–359. doi:10.2113/10.4.347
- Amadi AA, Eberemu AO (2013) Characterization of geotechnical properties of lateritic soil-bentonite mixtures relevant to their use as barrier in engineered waste landfills. *Nigerian J Technol* 32(1): 93–100. <http://nijotech.com/index.php/nijotech/article/view/618>. July 2014
- Barry DA, Parker JC (1987) Approximations to solute transport in porous media with flow transverse to layering. *Transp Porous Med* 2(1):65–82. doi:10.1007/BF00208537
- Brusseu ML (1992) Nonequilibrium transport of organic chemicals: the impact of pore-water velocity. *J Contam Hydrol* 9(4):353–368. doi:10.1016/0169-7722(92)90003-W
- Buragohain P, Sredeep S, Saiyouri N (2013) A study on the adsorption of ammonium in bentonite and kaolinite. *Int J Chem Environ Biolog Sci* 1(1):157–160. <http://www.isaet.org/images/extramages/IJCEBS%200101133.pdf>. July 2014
- Cameron DR, Klute A (1977) Convective-dispersive solute transport with a combined equilibrium and kinetic adsorption model. *Water Resour Res* 13(1):183–188. doi:10.1029/WR013i001p00183
- Coats KH, Smith BD (1964) Dead-end pore volume and dispersion in porous media. *Soc Petrol Eng J* 4(1):73–84. doi:10.2118/647-PA
- Cuthbert MO, Mackay R, Tellam JH, Thatcher KE (2010) Combining unsaturated and saturated hydraulic observations to understand and estimate groundwater recharge through glacial till. *J Hydrol* 391(3–4):263–276. doi:10.1016/j.jhydrol.2010.07.025
- DiCarlo DA (2013) Stability of gravity-driven multiphase flow in porous media: 40 years of advancements. *Water Resour Res* 49(8):4531–4544. doi:10.1002/wrcr.20359
- Eguchi S, Hasegawa S (2008) Determination and characterization of preferential water flow in unsaturated subsoil of Andisol. *Soil Sci Soc Am J* 72(2):320–330. doi:10.2136/sssaj2007.0042
- Essandoh HMK, Tizaoui C, Mohamed MHA, Amy G, Brdjanovic D (2011) Soil aquifer treatment of artificial wastewater under saturated conditions. *Water Res* 45(14):4211–4226. doi:10.1016/j.watres.2011.05.017
- Gaber HM, Inskeep WP, Wraith JM, Comfort SD (1995) Nonequilibrium transport of atrazine through large intact soil cores. *Soil Sci Soc Am J* 59(1):60–67. doi:10.2136/sssaj1995.03615995005900010009x
- Griffioen JW, Barry DA (1999) Centrifuge modeling of unstable infiltration and solute transport. *J Geotech Geoenviron* 125(7):556–565. doi:10.1061/(ASCE)1090-0241(1999)125:7(556)
- Griffioen JW, Barry DA, Parlange J-Y (1998) Interpretation of two-region model parameters. *Water Resour Res* 34(3):373–384. doi:10.1029/97WR02027
- Güngör K, Ünlü K (2005) Nitrite and nitrate removal efficiencies of soil aquifer treatment columns. *Turkish J Eng Env Sci* 29(3): 159–170. <http://journals.tubitak.gov.tr/engineering/issues/muh-05-29-3/muh-29-3-3-0408-2.pdf>. July 2014
- Guo L, Wagenet RJ, Hutson JL, Boast CW (1997) Nonequilibrium transport of reactive solutes through layered soil profiles with depth-dependent adsorption. *Environ Sci Technol* 31(8):2331–2338. doi:10.1021/es960944h
- Heatwole KK, McCray JE (2007) Modeling potential vadose-zone transport of nitrogen from onsite wastewater systems at the

- development scale. *J Contam Hydrol* 91(1–2):184–201. doi:10.1016/j.jconhyd.2006.08.012
- Hewitt J, Hunter JV, Lockwood D (1979) A multiorder approach to BOD kinetics. *Water Res* 13(3):325–329. doi:10.1016/0043-1354(79)90213-6
- Hill DE, Parlange J-Y (1972) Wetting front instability in layered soils. *Soil Sci Soc Am J* 36(5):697–702. doi:10.2136/sssaj1972.03615995003600050010x
- Hillel D, Baker RS (1988) A descriptive theory of fingering during infiltration into layered soils. *Soil Sci* 146(1):51–56. doi:10.1097/00010694-198807000-00008
- Jellali S, Diamantopoulos E, Kallali H, Bennaceur S, Anane M, Jedidi N (2010) Dynamic sorption of ammonium by sandy soil in fixed bed columns: evaluation of equilibrium and non-equilibrium transport processes. *J Environ Manag* 91(4):897–905. doi:10.1016/j.jenvman.2009.11.006
- Kamra SK, Lennartz B, Van Genuchten MT, Widmoser P (2001) Evaluating non-equilibrium solute transport in small columns. *J Contam Hydrol* 48(3–4):189–212. doi:10.1016/S0169-7722(00)00156-X
- Levine AD, Asano T (2004) Recovering sustainable water from wastewater. *Environ Sci Technol* 38(11):201A–208A. doi:10.1021/es040504n
- Li L, Barry DA, Culligan-Hensley PJ, Bajracharya K (1994) Mass transfer in soils with local stratification of hydraulic conductivity. *Water Resour Res* 30(11):2891–2900. doi:10.1029/94WR01218
- Li Z, Yue Q, Gao B, Wang Y, Liu Q (2012) Phosphorus release potential and pollution characteristics of sediment in downstream Nansi Lake, China. *Front Environ Sci Eng* 6(2):162–170. doi:10.1007/s11783-011-0313-7
- Lin C, Banin A (2005) Effect of long-term effluent recharge on phosphate sorption by soils in a wastewater reclamation plant. *Water Air Soil Pollut* 164(1–4):257–273. doi:10.1007/s11270-005-3540-3
- Ling G, El-Kadi AI (1998) A lumped parameter model for nitrogen transformation in the unsaturated zone. *Water Resour Res* 34(2):203–212. doi:10.1029/97WR02683
- MacQuarrie KT, Sudicky EA (2001) Multicomponent simulation of wastewater-derived nitrogen and carbon in shallow unconfined aquifers I: model formulation and performance. *J Contam Hydrol* 47(1):53–84. doi:10.1016/S0169-7722(00)00137-6
- Maraqqa MA (2001) Prediction of mass-transfer coefficient for solute transport in porous media. *J Contam Hydrol* 53(1–2):153–171. doi:10.1016/S0169-7722(01)00198-X
- McCray JL, Huntzinger DN, Van Cuyk S, Siegrist R (2000) Mathematical modeling of unsaturated flow and transport in soil-based wastewater treatment systems. *Proc Water Environ Fed.* doi:10.2175/193864700784608667
- Meneses M, Pasqualino JC, Castells F (2010) Environmental assessment of urban wastewater reuse: treatment alternatives and applications. *Chemosphere* 81(2):266–272. doi:10.1016/j.chemosphere.2010.05.053
- Mollins LH, Stewart DI, Cousens TW (1996) Predicting the properties of bentonite-sand mixtures. *Clay Miner* 31(2): 243–252. [http://www.minersoc.org/pages/Archive-CM/Volume\\_31/31-2-243.pdf?origin=publication\\_detail](http://www.minersoc.org/pages/Archive-CM/Volume_31/31-2-243.pdf?origin=publication_detail). July 2014
- Ollivier P, Surdyk N, Azaroual M, Besnard K, Casanova J, Rampnoux N (2013) Linking water quality changes to geochemical processes occurring in a reactive soil column during treated wastewater infiltration using a large-scale pilot experiment: insights into Mn behavior. *Chem Geol* 356:109–125. doi:10.1016/j.chemgeo.2013.07.023
- Panasiuk O (2010) Phosphorus removal and recovery from wastewater using magnetite. MSci Thesis, Royal Inst. Technology, Stockholm. <http://www.diva-portal.org/smash/record.jsf?pid=diva2:473397>. July 2014
- Pang L, Close M, Schneider D, Stanton G (2002) Effect of pore-water velocity on chemical nonequilibrium transport of Cd, Zn, and Pb in alluvial gravel columns. *J Contam Hydrol* 57(3–4):241–258. doi:10.1016/S0169-7722(01)00223-6
- Parkhurst DL, Appelo CAJ (1999) User's guide to PHREEQC (version 2): a computer program for speciation, batch-reaction, one-dimensional transport, and inverse geochemical calculations. [http://wwwbrr.cr.usgs.gov/projects/GWC\\_coupled/phreeqc/html/final.html](http://wwwbrr.cr.usgs.gov/projects/GWC_coupled/phreeqc/html/final.html). July 2014
- Parlange J-Y, Hill DE (1976) Theoretical analysis of wetting front instability in soils. *Soil Sci* 122(4):236–239. doi:10.1097/00010694-197610000-00008
- Rosqvist NH, Dollar LH, Fourie AB (2005) Preferential flow in municipal solid waste and implications for long-term leachate quality: valuation of laboratory-scale experiments. *Waste Manag Res* 23(4):267–380. doi:10.1177/0734242X05056995
- Saadi Z, Maslouhi A (2003) Modeling nitrogen dynamics in unsaturated soils for evaluating nitrate contamination of the Mnasra groundwater. *Adv Environ Res* 7(4):803–823. doi:10.1016/S1093-0191(02)00055-2
- Schmidt CM, Fisher AT, Racz AJ, Lockwood BS, Huertos ML (2011) Linking denitrification and infiltration rates during managed groundwater recharge. *Environ Sci Technol* 45(22):9634–9640. doi:10.1021/es2023626
- Selker JS, Steenhuis TS, Parlange J-Y (1992) Wetting front instability in homogeneous sandy soils under continuous infiltration. *Soil Sci Soc Am J* 56(5):1346–1350. doi:10.2136/sssaj1992.03615995005600050003x
- Shariatmadari H, Shirvani M, Jafari A (2006) Phosphorus release kinetics and availability in calcareous soils of selected arid and semiarid toposequences. *Geoderma* 132(3–4):261–272. doi:10.1016/j.geoderma.2005.05.011
- Sharpley AN, Ahuja LR, Yamamoto M, Menzel RG (1981) The kinetics of phosphorus desorption from soil. *Soil Sci Soc Am J* 45(3):493–496. doi:10.2136/sssaj1981.03615995004500030010x
- Singh N, Kloeppel H, Klein W (2002) Movement of metolachlor and terbuthylazine in core and packed soil columns. *Chemosphere* 47(4):409–415. doi:10.1016/S0045-6535(01)00322-8
- Smedt FDE, Wierenga PJ (1979) Mass transfer in porous media with immobile water. *J Hydrol* 41(1–2):59–67. doi:10.1016/0022-1694(79)90105-7
- Smedt FD, Wierenga PJ (1984) Solute transfer through columns of glass beads. *Water Resour Res* 20(2):225–232. doi:10.1029/WR020i002p00225
- Spiteri C, Slomp CP, Regnier P, Meile C, Van Cappellen P (2007) Modelling the geochemical fate and transport of wastewater-derived phosphorus in contrasting groundwater systems. *J Contam Hydrol* 92(1–2):87–108. doi:10.1016/j.jconhyd.2007.01.002
- Starr JL, Broadbent FE, Nielsen DR (1974) Nitrogen transformation during continuous leaching. *Soil Sci Soc Am J* 38(2):283–289. doi:10.2136/sssaj1974.03615995003800020023x
- Surridge BM, Heathwaite AL, Baird AJ (2007) The release of phosphorus to porewater and surface water from river riparian sediments. *J Environ Qual* 36(5):1534–1544. doi:10.2134/jeq2006.0490
- Tchobanoglous G, Burton FL, Stensel HD (2003) *Wastewater engineering: treatment and reuse*, 4th edn. McGraw-Hill, New York, pp 80–90
- Wassmann P, Olli K (eds) (2004) *Drainage basin nutrient inputs and eutrophication: an integrated approach*. University of Tromsø, Norway, 161 pp. <http://hdl.handle.net/10037/2389>. July 2014
- Yamaguchi T, Moldrup P, Rolston DE, Ito S, Teranishi S (1996) Nitrification in porous media during rapid unsaturated water flow. *Water Res* 30(3):531–540. doi:10.1016/0043-1354(95)00206-5
- Yao L, Feng S, Mao X, Huo Z, Kang S, Barry DA (2012) Coupled effects of canal lining and multi-layered soil structure on canal seepage and soil water dynamics. *J Hydrol* 430–431:91–102. doi:10.1016/j.jhydrol.2012.02.004
- Zhou L, Selim HM (2001) Solute transport in layered soils. *Soil Sci Soc Am J* 65(4):1056–1064. doi:10.2136/sssaj2001.6541056x